

Atomic mass of ${}^6\text{Li}$ using a Penning-ion-trap mass spectrometer

T. P. Heavner and S. R. Jefferts

Time and Frequency Division, National Institute of Standards and Technology, Boulder, Colorado 80305

G. H. Dunn

*JILA, University of Colorado and National Institute of Standards and Technology,
Boulder, Colorado 80309-0440*

(Received 6 June 2001; published 16 November 2001)

The atomic mass of ${}^6\text{Li}$ has been measured using a Penning-ion-trap mass spectrometer to be 6.015 122 795(16) u. The fractional measurement uncertainty of $\pm 2.7 \times 10^{-9}$ represents a 30-fold improvement over that of the accepted published value. External ion sources were used to create ions outside the cryogenic (4 K) environment of the Penning trap and an ion-transport beamline was used to deliver ions into the trap for measurement. The ion mass ratios of ${}^6\text{Li}^+ : {}^{12}\text{C}^{2+}$ and ${}^6\text{Li}^+ : \text{D}_3^+$ were measured using this apparatus and the atomic mass of neutral ${}^6\text{Li}$ was derived from these ratios. A measurement of the $\text{He}^+ : \text{D}_2^+$ mass ratio with a fractional uncertainty of $\pm 1.1 \times 10^{-9}$ and differing from the accepted published value by a fractional amount -0.6×10^{-9} is also reported.

DOI: 10.1103/PhysRevA.64.062504

PACS number(s): 32.10.Bi, 07.75.+h, 21.10.Gv, 06.20.Jr

I. INTRODUCTION

A thrust has developed in recent years for higher accuracy atomic mass measurements with motivation [1] ranging from an atomic mass standard to relevance to fundamental constants, and touching many other areas in between. For example, imprecise knowledge of the mass of ${}^6\text{Li}$ treated in this paper has been [2] in the past one limiting factor in the search for parity nonconservation.

Penning ion traps have become a key tool in obtaining these highly accurate atomic-mass measurements, and some groups now achieve single-ion-mass measurements with uncertainties of parts in 10^{10} . Many of the techniques employed by these groups are derived from the work of Dehmelt and his colleagues aimed at measuring $g-2$ for a single electron confined in a Penning trap [3,4]. Van Dyck's group [5] developed techniques to trap and detect ions by observing image currents induced in the trap electrodes by the oscillating ions, and measured several light-ion masses with an uncertainty of a few parts in 10^{10} , and Van Dyck has recently talked about measurements a factor of ten more accurate than that [6]. Pritchard's group at MIT [7] developed a related Penning-ion-trap mass spectrometer and has achieved uncertainties of a few parts in 10^{10} for a number of species with masses of ≈ 10 u to ≈ 133 u, the higher masses being reported recently with an accuracy of one part in 10^{10} [8]. Bergstrom's group in Stockholm [9] uses a time-of-flight scheme, originally developed at the Johannes Gutenberg-Universität at Mainz [10], incorporating a Penning trap to measure cyclotron resonances. The Stockholm experiment, termed SMILETRAP, can use highly charged ions created in an electron beam ion trap (EBIS) ion source that are subsequently injected into the trap for measurement, or alternatively can inject singly charged ions (e.g., H_2^+) from a simple ion source. Using highly charged ions introduced from outside the trap region offers the flexibility to make measurements over a much broader range of species and mass than the other methods. Uncertainties of 1 ppb [11] and now a few

parts in 10^{10} have been achieved [12]. The Mainz group has also continued to refine their technique and have recently reported [13] measurements on several light ions (including He^+ and D_2^+) with inaccuracies as low as five parts in 10^{10} .

We developed a Penning-ion-trap mass spectrometer incorporating many of the features found in these other experiments with the goal of measuring atomic masses with uncertainties of less than 1 part in 10^9 [14–17], a goal that was only approached—as reported herein—before the apparatus was dismantled and the experiments discontinued. Despite not reaching state-of-the-art accuracies achieved by some others, the results reported here for ${}^6\text{Li}$ at an accuracy of 2.7 ppb represent a 30-fold increase in accuracy for this species. Our system combined external ion-loading capabilities as used by the Stockholm group with a sensitive single-ion-detection scheme similar to those used in the Van Dyck and Pritchard experiments, and some features of the system and its operation are of particular interest.

II. EXPERIMENT

Penning traps—review and application

The physics of a single electron or ion in a Penning trap is thoroughly treated by Brown and Gabrielse [18], and much of the following discussion is found in more detail in their paper. Consider the schematic diagram of a Penning ion trap shown in Fig. 1. The trap consists of five electrodes: the ring, two endcaps, and a pair of compensation or guard ring elec-

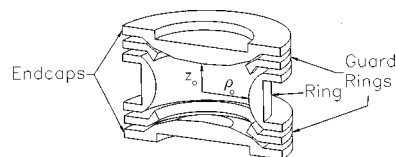


FIG. 1. Schematic diagram of a Penning ion trap. The dimensions of the trap described here are $z_0 = 0.603$ cm and $\rho_0 = 0.700$ cm.

trodes. The ring and endcaps are machined as hyperbolas of revolution forming equipotential surfaces of an electrostatic quadrupole potential. An ion is confined in the z or axial direction by the quadrupole electric field created by the trap electrodes. However, the force on the ion due to the radial component of this field pushes the ion out of the trap radially. A strong magnetic field superimposed on the trap in the axial direction completes the confinement in all three dimensions.

The resulting motion of a single ion in an ideal Penning ion trap is the superposition of three modes of oscillation. First, the ion undergoes simple harmonic motion in the axial direction with a frequency ω_z given by

$$\omega_z = \sqrt{\frac{qV_0}{md_0^2}}, \quad (1)$$

where q is the charge on the ion, m is the ion mass, V_0 is the potential difference between the endcaps and the ring electrode, and d_0 is a characteristic trap dimension as defined in Ref. [18].

In the radial direction ρ the motion is the superposition of two modes. These modes oscillate at the modified cyclotron frequency ω'_c and the much lower magnetron frequency ω_m , which are given by

$$\begin{aligned} \omega'_c &= \frac{1}{2}(\omega_c + \sqrt{\omega_c^2 - 2\omega_z^2}), \\ \omega_m &= \frac{1}{2}(\omega_c - \sqrt{\omega_c^2 - 2\omega_z^2}), \end{aligned} \quad (2)$$

where ω_c is the free space cyclotron frequency given by

$$\omega_c = \frac{qB}{m}. \quad (3)$$

The Penning ion trap normally operates in the regime such that $\omega'_c \gg \omega_z \gg \omega_m$. In our experiment, $\omega'_c \approx (2\pi)18$ MHz, $\omega_z \approx (2\pi)1$ MHz, $\omega_m \approx (2\pi)23$ kHz with the operating parameters of $B \approx 7$ T, $d_0 = 0.5516$ cm and $V_0 \approx -60$ V for an ion with m/q of $6u/e$.

Brown and Gabrielse developed an invariance relationship [18]

$$\omega_c^2 = \omega'^2_c + \omega_z^2 + \omega_m^2, \quad (4)$$

which provides a robust recipe for recovering the free-space cyclotron frequency from the frequencies of the three trap modes. This relationship is invariant under perturbations due to misalignment of the trap's z axis with the trapping magnetic field and ellipticity in the trap electrodes due to machining imperfections. Equation (4) also gives a prescription for the uncertainty needed in the measurement of each frequency in order to obtain the free-space cyclotron frequency at the desired level of accuracy.

If the free-space cyclotron frequency for ion 1 with mass m_1 and charge q_1 is measured at time t_1 to be $\omega_{c1}(t_1)$ and the free-space cyclotron frequency for ion 2 with mass m_2

and charge q_2 is measured at a later time t_2 to be $\omega_{c2}(t_2)$, then the mass ratio of the two ions is

$$\frac{m_2}{m_1} = \frac{\omega_{c1}(t_1)q_2B(t_2)}{\omega_{c2}(t_2)q_1B(t_1)}. \quad (5)$$

In an ideal experiment, the magnetic field sampled by the ions does not change with time. However, in reality, the measurement uncertainty is often dominated by drifts and fluctuations in the magnetic field, and it is, therefore, necessary to develop techniques to characterize the drift and noise of the magnetic field. For example, performing a sequence of alternate measurements on ion 1 and ion 2 allows the magnetic field to be measured as a function of time allowing for this drift to be removed from the data. Magnetic-field variations can be due to noise in the external field in the laboratory or from drift in the trapping field.

The trap modes of oscillation given by Eq. (1) through Eq. (3) are for the case of a single ion in an ideal trap. In reality, the motion of an ion in a Penning trap differs from that discussed due to imperfections in the trapping potentials as well as relativistic effects. In fact, these perturbations are central to the cyclotron resonance scheme used in this work. These frequency shifts must be considered in precision measurements using Penning traps and have earlier been discussed by Brown and Gabrielse [18]. The advantage of measuring mass ratios of *doublets* and using single ions is that these shifts are approximately the same for both ions and cancel, to a large extent, in the ratio. Experimentally, we always attempt to operate the apparatus using a single ion at a time. However, due to difficulties of consistently loading single ions, the data presented in this paper result from cases in which the number of ions confined in the trap varied from 1 to approximately 10 between successive ion loads. This results in an ion-number-dependent systematic bias that is removed from the data. This is discussed in more detail in Sec. III of the paper.

Following Ref. [18], if the trap electrostatic potential is expanded in Legendre polynomials, the ideal trap potential is given by the second-order term. The most significant electrostatic perturbation is described by the fourth-order term, the strength of which is characterized by a dimensionless parameter C_4 . (The odd-order terms are negligible due to azimuthal symmetry). This perturbation adds an anharmonic potential which has the characteristic that the axial resonance frequency shifts proportional to the square of the amplitude of oscillation. This anharmonicity is controlled to a large extent by applying a voltage on the guard ring electrodes and is nulled out to $|C_4| \lesssim 5 \times 10^{-6}$. In this work, the residual C_4 leads to systematic shifts in the measured mass ratios of order 1 part in 10^{10} . These shifts are uncorrected for in our final results.

Similarly, the trapping magnetic field can be described [18] by an expansion in Legendre polynomials. The most significant magnetic-field perturbation to the desired uniform trapping field is the second-order term that is representative of a magnetic bottle described in strength by the parameter B_2 . This causes the cyclotron frequency to shift proportional to the square of the radial amplitude. This bottle term is

minimized by the use of a high-quality superconducting magnet system equipped with gradient shimming coils and by careful selection of low-magnetic-susceptibility materials used in the construction of the trap and the neighboring components in the vacuum system. The residual B_2 is ≈ 0.33 T/m², and systematic shifts in the measured mass ratios due to this term are removed in the data analysis.

The linear magnetic-field gradient B_1 alone causes no net shift in the cyclotron frequency, since the field due to this term as seen by the ion averages to zero over one orbit. However, in the presence of patch potentials on the trap electrodes, two different ions will reside in different equilibrium positions within the trap (since the ring potential is slightly different in order to bring the two ions into resonance with the axial detector) and the magnetic field will differ by the amount of B_1 times the displacement between the equilibrium positions. In our experiment we have minimized this problem by several means. First, since our trap is relatively large ($d_0 = 0.5516$ cm) and operates with approximately -60 V on the ring at mass 6 u, the effect of patches is not as severe as it would be if it were a smaller trap operating at a lower ring voltage. Also, we coated the trap electrodes with graphite (Aerodag), which has been shown to reduce patch potentials in other Penning traps [19]. In our apparatus, this gradient was measured to be $|B_1| \leq 3$ G/cm by applying a dc potential on one endcap, thus shifting the equilibrium position of the ion in the z direction, and then measuring the resulting shift in the cyclotron frequency. A patch causing a ≈ 1 V difference between the two endcaps (considered extremely unlikely) would be needed to cause a shift of 1×10^{-9} in a measurement of doublets with $(\Delta m/m) = 5 \times 10^{-3}$.

The third major deviation from the ideal trap frequencies is due to relativistic mass increases arising from the increased energies from the excitation drives. These shifts also scale as the squares of the amplitudes of oscillation and again are negligible in the measurement of the mass doublets presented here.

JILA Penning trap—details

Details of the JILA Penning ion trap used in these measurements have been discussed elsewhere [14–17]. The trap is a compensated, hyperbolic design and is machined to high tolerances from a copper-nickel alloy [14], which exhibits a magnetic susceptibility approximately ten times smaller than that of oxygen-free high-conductivity copper (OFHC) at 4 K. The trap is enclosed within a vacuum insert that is likewise constructed from OFHC and other materials with low magnetic susceptibilities. During operation, the insert is located within the liquid He-cooled bore of the 7 T trapping magnet. The top of the insert is outside of this dewar and contains various feedthroughs to send signals to and from the trap. Also residing within the insert is an ion-transport beamline and various focusing, steering, and deceleration optics used to help deliver ions from the external sources into the trap. A miniature gate valve located on the top of the insert allows

for this insert to be connected to an external vacuum system containing ion sources and additional ion-beam transport optics.

Loading ions into the Penning trap from the external ion sources was a challenging task. The details of the ion sources, beam transport lines, and alignment technique are too cumbersome to present in this paper but are found in Ref. [17]. Here we discuss some features of the system that we found to be helpful in achieving the task of loading ions. Other details are particular to our design and laboratory constraints and do not necessarily constitute the ideal system. Many other ion source and ion-delivery systems may work just as well or better in other experimental configurations.

Two different ion sources and ion-delivery systems were used in the measurements presented here. A commercial plasma discharge source was used to create D_2^+ , D_3^+ , He^+ , and ${}^{12}\text{C}^+$ from various parent gases introduced into the source. In the case of ${}^{12}\text{C}^{2+}$, singly charged ${}^{12}\text{C}^+$ was loaded into the trap and subsequently doubly ionized using an electron gun located below one trap endcap. Ions from the source were mass selected using an $\mathbf{E} \times \mathbf{B}$ velocity filter and transported through a beamline to the top of the Penning-trap insert. The beamline contained several stages of deflection plates and focusing optics sufficient to have control over all the degrees of freedom of the ion-beam trajectory. An electrostatic quadrupole bender was used to deflect the ion beam 90° down into the trapping magnetic field and towards the Penning trap. The ${}^6\text{Li}^+$ ions were obtained from a $\text{Li}_2\text{O} \cdot \text{Al}_2\text{O}_3 \cdot 4\text{SiO}_2$ (spodumene) solid-emitter-type source. This source and associated extraction and focusing optics were mounted on top of the Penning-trap insert such that the beam axis was coaxial with the Penning-trap z axis. This geometry did not require the use of the quadrupole bender. Also, because of the purity of the beam from the ${}^6\text{Li}^+$ emitter, we did not mass select the ion beam. Switching between ion sources was accomplished by simply changing a few voltages and did not significantly contribute to the dead time between ion-ion comparisons.

The difficulty of transporting ions from the top of the insert and into the trap derives primarily from the presence of the large magnetic-field gradients that tend to reflect the beam backwards. Steering the beam into the trap using only electrostatic methods proved ineffective. It was crucial to first carefully align the axis of the trap and the ion-transport optics with the axis of the magnetic field before ions could be successfully loaded into the trap. An electron gun located below the Penning trap was used as a powerful alignment tool. We monitored the amount of current from this electron gun passing through the apertures in the trap endcaps, out of the magnetic-field gradient and onto a collector near the top of the insert while adjusting the location and angle of the insert assembly with respect to the trapping magnetic field with angular tolerances of $\approx 10^{-4}$ rad. Maximizing the current to this collector outside of the strong field region resulted in the system being well aligned, and the ion beam was then easily directed into the trap with minor beam steering and additional mechanical adjustments [17].

Once an ion beam is directed into the trap, loading was achieved using a multistep process. First, a “catch” trap con-

sisting of the measurement trap electrodes plus an additional available electrode below the lower endcap is used to trap a large number (≈ 1000) of ions from the beam. Thus the catch trap overlaps the measurement trap in the axial direction. The ions in the catch trap undergo ion-ion collisions and equilibrate in about 10 s. Reducing the potential on the catch trap leads to evaporative cooling of the sample leaving a small number (typically 1–10) remaining within the boundaries of the measurement trap.

Measurement of the axial resonance frequency is accomplished by detecting the image currents induced in one endcap by the oscillating ions [3]. A high- Q ($Q \approx 15\,000$) LC circuit resonant at $\omega_T \approx \omega_z \approx (2\pi)1$ MHz is connected between the lower endcap and ground. On resonance, the impedance of the tuned circuit is real and has a value of $R \approx Q\omega L \approx 57\text{ M}\Omega$. The ion image currents create a voltage across this resistance that is amplified and mixed down to a dc error signal using a version of the sideband detection scheme developed by Wineland, Ekstrom, and Dehmelt [4]. The energy dissipated in the external circuit comes from the ions' motion, so that the axial motion of the ions is damped at a rate γ_z given by

$$\gamma_z = N_{\text{ions}} \left(\frac{qC_1}{2z_0} \right)^2 \frac{Q\omega L}{m}, \quad (6)$$

where N_{ions} is the number of ions in the trap. Hence, a measurement of the linewidth of the axial response provides a means to monitor the number of ions in the trap.

Amplitude-dependent frequency shifts due to imperfections in the trapping fields and relativistic effects provide a means to detect excitation of the radial modes of oscillation by monitoring shifts in the axial mode. If the frequency of the axial motion is servo locked to the ring voltage, then a small change in the radial amplitude of the ion can be detected by observing a change in the correction voltage applied to the ring electrode. Coupling of the radial and axial modes is also accomplished by applying an rf quadrupole field across the center of the trap. Sideband cooling [20] is used to minimize the amplitudes of the magnetron and cyclotron orbits both after loading and after the heating associated with cyclotron frequency determinations.

Cyclotron resonances

In line with the above discussion, the trap cyclotron frequency is thus measured by phase locking the axial motion and applying an rf potential across the trap. The rf potential is swept in frequency across the trap cyclotron frequency ω'_c . On resonance, the ion's cyclotron orbit increases resulting in a shift in the axial frequency due to the anharmonic perturbations. A typical trap cyclotron resonance obtained in our apparatus is shown in Fig. 2 where phase-lock correction voltage is plotted versus frequency of the applied rf field.

Low-frequency beats similar to those which appear in the cyclotron scan in Fig. 2 were first observed in ion-trap mass spectrometry by Van Dyck's group. Moore *et al.* [21] kept the frequency of the excitation oscillator fixed while they observed the low-frequency beat between the ion and the

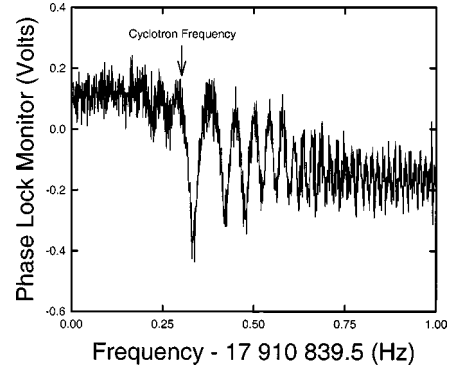


FIG. 2. A cyclotron resonance obtained on a single D_3^+ ion in our trap. The x axis is the frequency of the cyclotron excitation oscillator and the y axis shows the axial motion phase-lock correction voltage monitor. The correction voltage monitor is ≈ 1000 times the correction voltage added to the ring and has a ≈ 1 Hz filter on the output.

oscillator for a long period of time. They proposed that by recording this low-frequency beat and taking the cyclotron resonance frequency as the difference between this frequency and the applied oscillator frequency, the cyclotron frequency could be determined to very high resolution (parts in 10^{11}).

Van Dyck *et al.* [5] discuss the shape of such resonances when the excitation oscillator is swept up and down in frequency around the resonance. On an upswept resonance, an abrupt steplike transition is followed by beats such as those observed here. Once the ion has been excited, it is out of resonance with the applied drive and the two frequencies beat together. On a down swept resonance, the applied drive stays in resonance with the shifted cyclotron resonance as a result of the relativistic mass increase and continues to drive the ion to larger cyclotron amplitudes.

In such precision measurements, it is important to understand the physics of these complex lineshapes so that they can be interpreted accurately and meaningful measurements extracted from the data. The following simple model of this system provides further insight into this cyclotron resonance lineshape and is useful in identifying the cyclotron frequency from the structure of the resonance lineshape.

Consider a trapped ion being driven close to the cyclotron frequency by an electric dipole field across the center of the trap. Since the damping time constant for a trapped ion undergoing cyclotron motion at 18 MHz is about 10^4 year, the system can be treated as a driven, undamped slightly anharmonic oscillator. Thus, the sum of the forces acting on the ion is

$$q\mathbf{v} \times \mathbf{B} + q\mathbf{E}_T + q\mathbf{E}_d \cos(\omega_d t) = m\mathbf{a}, \quad (7)$$

where \mathbf{B} is the trapping magnetic field, \mathbf{E}_T is the trapping electric field, and \mathbf{E}_d is the driving dipole field at frequency ω_d across the center of the trap and perpendicular to \mathbf{B} . Experimentally, the ω_d excitation drive is applied across the two halves of the upper guard ring electrode, which has been split into two symmetric pieces for this purpose. Following arguments given by Brown and Gabrielse [18], we simplify

the problem by neglecting the radial component of the electric field and replace the free-space cyclotron frequency ω_c with the trap cyclotron frequency ω'_c . Using Cartesian coordinates and taking the cyclotron motion to be in the x - y plane with the electric driving field to be in the x direction, we can separate Eq. (7) into the pair of coupled equations

$$\begin{aligned} \frac{d^2x}{dt^2} - \omega'_c \frac{dy}{dt} - \frac{qE_d}{m} \cos(\omega_d t) &= 0, \\ \frac{d^2y}{dt^2} + \omega'_c \frac{dx}{dt} &= 0. \end{aligned} \quad (8)$$

This pair can be combined and simplified to yield an expression that describes $dy(t)/dt$ in terms of a driven, undamped simple harmonic oscillator. The solution for $dy(t)/dt$ is found by performing the convolution of the ‘‘chirped’’ forcing function with the Green’s function for the harmonic oscillator [17]. The result can be simplified in such a way that the fast motion at the cyclotron frequency ω'_c is separated from the evolution of the amplitude envelope resulting in

$$\begin{aligned} dy(t)/dt &= \frac{E_d}{m} \cos\left(\omega'_c t - \left(\frac{\omega_s - \omega'_c}{\alpha}\right)^2\right) \int_0^t \cos\left(t' \sqrt{2\alpha}\right. \\ &\quad \left. + \sqrt{\frac{2}{\alpha}}(\omega_s - \omega'_c)\right)^2 dt', \end{aligned} \quad (9)$$

where ω_s and α are defined in the expression for the instantaneous frequency of the forcing function

$$\omega_d(t) = \omega_s + \frac{1}{2} \alpha t. \quad (10)$$

The first cosine term in Eq. (9) contains the information describing the fast part of the cyclotron motion. The second term, the integral of a cosine with a squared argument (Fresnel integral), describes the slow evolution of $dy(t)/dt$.

This Fresnel integral was evaluated numerically using typical experimental parameters and the results, shown in Fig. 3, can be used to interpret the lineshape of an actual cyclotron resonance (Fig. 2). The upper plot in Fig. 3 displays the cyclotron orbit radius as a function of time where the 1 Hz frequency sweep lasting 100 s is started 0.5 Hz below the cyclotron resonance. This plot shows that the ion beats with the applied drive before resonance causing the radius of the cyclotron orbit to fluctuate in magnitude. Upon passage through the ion cyclotron resonance, the radius of the orbit increases to ≈ 0.2 mm. Above the resonance frequency, the ion continues to beat with the applied excitation drive causing the orbit radius to again fluctuate in magnitude. The lower plot displays how this resonance appears when observed through the axial lock (assuming typical anharmonicity parameters used in our apparatus). Since the axial lock signal is proportional to ρ_c^2 , the resonance lineshape acquires a nonlinear structure. This demonstrates that we should not assign the cyclotron resonance to the point at which the axial lock begins to shift levels. A linear extrapolation of the slope

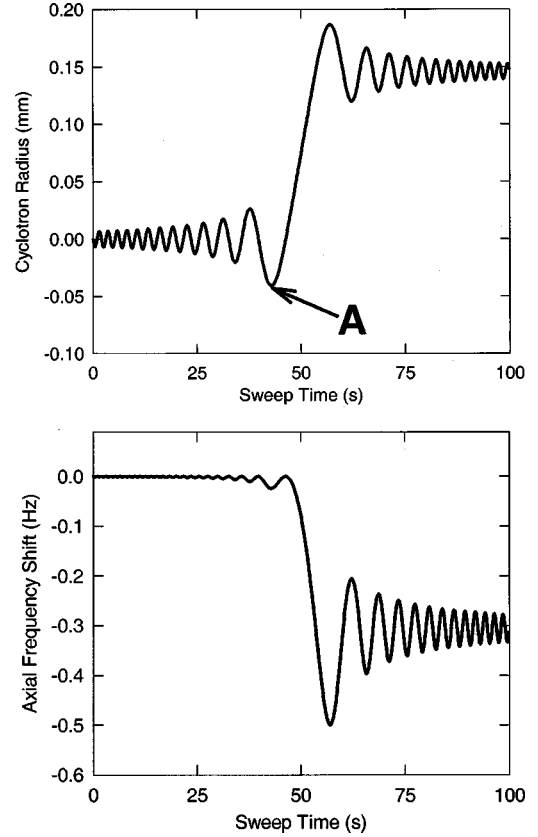


FIG. 3. Simulation of the driven ion cyclotron resonance. The upper plot displays the cyclotron orbit radius as a function of time where the 1 Hz wide frequency sweep lasting 100 s is started 0.5 Hz below the resonance. The lower plot displays this cyclotron resonance as detected by the axial lock. Since the axial frequency shift is proportional to ρ_c^2 , the detected beats are larger after passing through resonance. The feature labeled A in the upper plot corresponds to the point at which turning off the excitation drive leaves the cyclotron orbit in a subthermal state.

of the steplike transition to the intercept with the baseline provides yet a better estimate of the cyclotron frequency. Nevertheless, the *absolute* cyclotron frequency will be located at a point along the transition in the axial lock that depends on the anharmonicity parameters. Furthermore, the lineshape structure can be tuned with C_4 and B_2 . In this simulation, the true cyclotron resonance at $t = 50$ s is close to the point at which the dc level of the lock signal begins to change but it is shifted by approximately 20 mHz, which is about a 1 part in 10^9 shift at a cyclotron frequency of 18 MHz. These lineshape effects are, therefore, very important when trying to extract *absolute* frequency measurements from the data or in the case of measuring ratios of nondoublets. When one is measuring frequency ratios, as in the case of investigating mass doublets, as long as one picks the same feature in the lineshape for each member of the doublet, the error introduced by the offset of the feature from the true cyclotron frequency is negligible. In the results presented here with doublets of mass 6 u differing by $\Delta m/m \approx 10^{-2}$, the resulting error from choosing the same feature in the lineshape as defining the resonance is $\leq 10^{-11}$.

The low-frequency behavior of the cyclotron radius could conceivably also be used as a tool to prepare an ion with a subthermal cyclotron radius. For example, turning off the rf drive field at the point labeled **A** in Fig. 3 would leave the ion with a cyclotron radius smaller than its original, thermal value.

III. MEASUREMENTS AND DATA ANALYSIS

The mass ratios, ${}^6\text{Li}^+:\text{D}_3^+$, ${}^6\text{Li}^+:{}^{12}\text{C}^{2+}$, and $\text{He}^+:\text{D}_2^+$, were measured during experimental runs over approximately 1 yr. Both ion-trap cyclotron frequency and axial-frequency values were obtained versus time in each run. A fitting routine that determined the best cyclotron frequency ratio (or equivalently the best mass ratio between the ions compared during the run), and the best set of coefficients describing the linear drift in the magnetic field during the experimental run was used.

Systematic corrections

When comparisons of frequency measurements are made for single ions of mass doublets, systematic shifts largely cancel, provided that both ions are excited to the same amplitude, sample the same field perturbations, and undergo the same relativistic shifts. However, in the data presented here, two factors prevent us from using this cancellation argument. Ideally, measurements are made by comparing the cyclotron frequencies of single ions; however, numerous difficulties with our experimental apparatus prevented us from always operating under this condition. Thus, the number of ions measured in our data varies from one to approximately ten. Since the interaction of trapped ions with the high- Q circuit used to detect the axial mode depends on the total mass, ten ions will have 1/10 the axial amplitude of a single ion when driven with the same axial excitation signal. Another concern is related to the trapping of multiply charged ions. Although the ion ${}^{12}\text{C}^{2+}$ has the same mass-to-charge ratio as ${}^6\text{Li}^+$, their motions are not equivalent within the ion trap. Since the axial damping rate is proportional to q^2/m , a single ${}^{12}\text{C}^{2+}$ ion will have half the axial amplitude as a single ${}^6\text{Li}^+$ ion for the same axial excitation drive voltage. One approach is to adjust the rf excitation levels according to the number of ions and the ion charge state to cancel these effects. We did not use this technique because of our particular experimental configuration and we, therefore, had to correct for these effects in the data analysis.

A variety of other systematic shifts were considered in the data analysis and we determined that they are negligible at the level of the results presented here. These include a shift due to the low-frequency modulation of the trap potential used in the detection system, the shift due to the interaction of the ions with the high- Q tuned circuit (tuned-circuit pulling), and the uncertainty that arises from using the invariance relationship to determine the magnetron frequency. The fractional frequency shifts from these effects are all $< 4 \times 10^{-11}$ and are described in detail in Ref. [17].

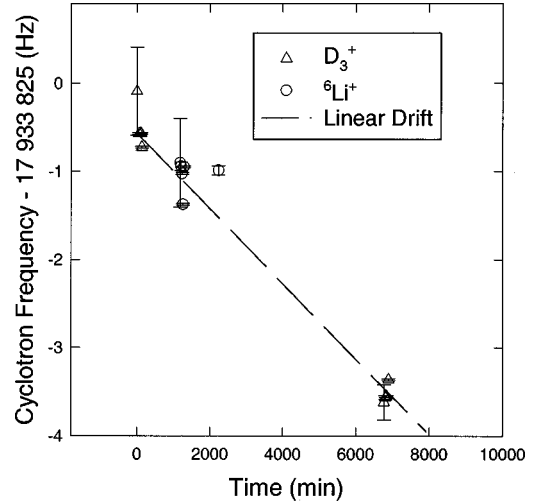


FIG. 4. A plot of a series of cyclotron measurements for D_3^+ and ${}^6\text{Li}^+$. The data are obtained by multiplying one set of cyclotron frequencies by the mass ratio derived from the fit such that all of the data can be plotted on the same graph. The dashed line is the linear magnetic field drift obtained from the fit. The error bars are the measurement uncertainties σ_m for each scan.

Magnetic bottle

The measured trap cyclotron frequency depends on the amplitude of the ion's axial motion, and the shift is given by [18]

$$\frac{\Delta\omega'_c}{\omega_c} = \frac{B_2}{2B_0} z^2. \quad (11)$$

The magnetic bottle strength B_2 was measured to be 0.33 T/m^2 . The term given by Eq. (11) dominates all other amplitude-dependent frequency shifts in our experiment, but cancels to a high degree in the mass ratio of single, mass doublet ions, as was the case for many of our measurements. However, in the cases where comparisons were made on different numbers of ions or charge states, this amplitude-dependent shift was accounted for in the final data analysis by using the knowledge of B_2 and the axial drive voltages.

Magnetic-field drift

Having obtained the free ion cyclotron frequencies ω_c from ω'_c , ω_z , and $\omega_m = \omega_z^2/2\omega'_c$ using Eq. (4) and correcting them for effects described above, we then have to compare ions measured at different times knowing that the magnetic field has changed. In the analysis of our data, only linear drifts in the magnetic field are considered. Higher-order fluctuations are present, but given the rather long ion loading time (\sim hours) inherent with our apparatus (and consequently a low-frequency sampling rate of the field), we feel this allows for only low-order estimates of the field drift. This lack of knowledge of the field drift directly translates into the dominant uncertainty in our final results.

An example of a typical resulting plot of free-space cyclotron frequency versus time for one run is shown in Fig. 4. The data are plotted by multiplying one of the two sets of

TABLE I. A summary of the mass ratio measurements from this work. The numbers in the parentheses indicate the uncertainty in the rightmost figures and represent one standard deviation.

Date	Ion 1	Ion 2	Magnetic field drift from the fit (Hz/min)	Mass ratio of ion 2 to ion 1 from the fit	Mass ratio of ion 2 to ion 1 calculated from masses in Ref. [22]
3/5/97	D_3^+	${}^6\text{Li}^+$	-4.27×10^{-4}	0.995 500 895 0(66)	0.995 500 802(84)
3/16/97	${}^{12}\text{C}^{2+}$	${}^6\text{Li}^+$	-8.42×10^{-4}	1.002 520 699 0(86)	1.002 520 608(85)
5/12/97	${}^{12}\text{C}^{2+}$	${}^6\text{Li}^+$	$+2.77 \times 10^{-4}$	1.002 520 691 2(38)	1.002 520 608(85)
10/19/97	${}^{12}\text{C}^{2+}$	${}^6\text{Li}^+$	$+5.21 \times 10^{-5}$	1.002 520 693 5(56)	1.002 520 608(85)
11/10/96	D_2^+	He^+	$+5.95 \times 10^{-4}$	0.993 643 871 2(11)	0.993 643 841 83(48)

cyclotron frequencies by the mass ratio that was obtained from the fitting procedure. This allows both sets of cyclotron frequencies to appear with the same y axis. The linear drift obtained from the fit has not been removed from the plotted frequencies. Rather, the linear drift is plotted along with the cyclotron frequencies and is shown by a dashed line. The error bars plotted here are the measurement uncertainties for each individual cyclotron scan and were used as the weighting factors in the determination of the mass ratio and the linear field drift.

IV. RESULTS OF THE MEASUREMENTS

The results for the comparison of ${}^6\text{Li}^+$ with the mass doublets D_3^+ and ${}^{12}\text{C}^{2+}$ and the comparison of D_2^+ with He^+ are summarized in Table I. The experimentally determined ion mass ratios presented here are compared to ion mass ratios calculated from neutral atomic masses published by Audi and Wapstra [22] (referred to here as AW). Ionization energies and molecular binding energies were taken from standard tables [23].

Figure 5 is a plot of the results for the ${}^6\text{Li}^+$ measurements presented in Table I and shows the fractional shifts between

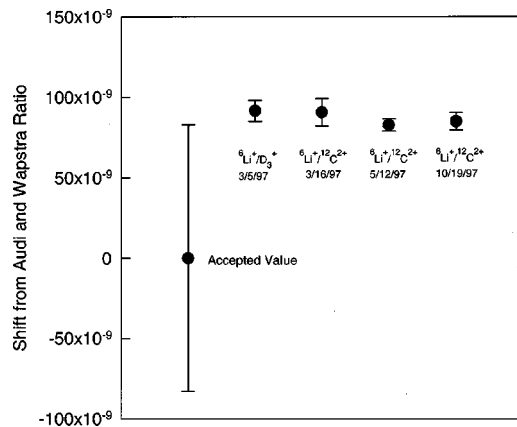


FIG. 5. A summary of the ${}^6\text{Li}^+$ mass measurements. The ratios measured in this work are plotted in terms of a fractional shift away from the presently accepted mass ratio.

the measured mass ratios and mass ratios calculated from the AW table. The first point, at zero on the y axis, represents the AW ratios and has an uncertainty that is always dominated by the uncertainty in the mass of ${}^6\text{Li}^+$. The remaining points are the results of this work and are presented in chronological order of experimental run from left to right.

Between the March and May measurements, the Penning-trap insert was removed from the LHe dewar for repairs. Also, before the October measurement, the trap was disassembled, cleaned, and reassembled. These measurements are all consistent despite the disruptive history of the apparatus.

The $\text{He}^+:\text{D}_2^+$ ratio presented here differs from the AW ratio by -0.6×10^{-9} . Figure 6 compares our measurement of the $\text{He}^+:\text{D}_2^+$ mass ratio with recent results from Van Dyck's [24] and Werth's [13] group and shows good agreement between all three results and the accepted value.

To obtain a value for the mass of neutral ${}^6\text{Li}$ from our work, the measured mass ratios were converted into neutral masses and a weighted mean was calculated. The final result for our value of the mass of neutral ${}^6\text{Li}$ is $6.015\,122\,795(16)$ u. The number in parentheses indicates the uncertainty in the rightmost figure and represents one standard deviation. The

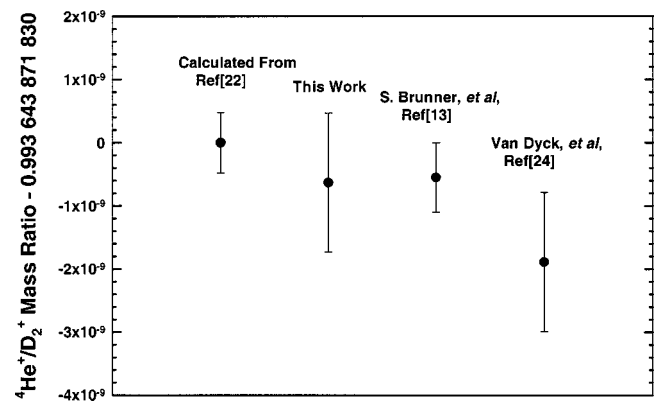


FIG. 6. A plot comparing the $\text{He}^+:\text{D}_2^+$ mass ratio presented in this work with other results. The first point on the left is the $\text{He}^+:\text{D}_2^+$ mass ratio calculated from the neutral masses tabulated in Audi and Wapstra (Ref. [22]). The rightmost two points are Penning-trap measurements from the Werth (Ref. [13]) and Van Dyck (Ref. [24]) groups.

mass of ${}^6\text{Li}$ in the AW table is 6.015 122 3(5) u, resulting in a difference between our mass value and the AW value of $+4.95 \times 10^{-7}$ u. The fractional uncertainty of our mass measurement is 2.7×10^{-9} versus 85×10^{-9} in the AW ${}^6\text{Li}$ mass.

ACKNOWLEDGMENT

This work was supported in part by the National Science Foundation under Grant No. PHY95-12150.

-
- [1] F. DiFilippo, V. Natarajan, M. Bradley, F. Palmer, and D. E. Pritchard, in *Atomic Physics 14*, edited by D. J. Wineland, C. E. Wieman, S. J. Smith, AIP Conf. Proc. No. 323 (AIP, New York, 1995), p. 149.
- [2] R. G. H. Robertson, J. A. Nolen, T. Chapuran, and R. Vodhanel, *Phys. Rev. C* **23**, 973 (1981).
- [3] H. G. Dehmelt and F. L. Walls, *Phys. Rev. Lett.* **21**, 127 (1968).
- [4] D. Wineland, P. Ekstrom, and H. Dehmelt, *Phys. Rev. Lett.* **31**, 1279 (1973).
- [5] For a summary of many measurements and discussion, see R. S. Van Dyck, Jr., D. L. Farnham, and P. B. Schwinberg, *Phys. Scr.* **T59**, 134 (1995).
- [6] R. S. Van Dyck, Jr., D. L. Farnham, S. L. Zafonte, and P. B. Schwinberg, in *Trapped Charged Particles and Fundamental Physics*, by Daniel H. E. Dubin and Dieter Schneider, AIP Conf. Proc. No. 457 (AIP, New York, 1999), p. 101.
- [7] For a summary of many measurements and discussion, see F. DiFilippo, V. Natarajan, M. Bradley, F. Palmer, and D. E. Pritchard, *Phys. Scr.* **T59**, 144 (1995).
- [8] M. P. Bradley, J. V. Porto, S. Rainville, J. K. Thompson, and D. E. Pritchard, *Phys. Rev. Lett.* **83**, 4510 (1999).
- [9] H. Borgenstrand, C. Carlberg, G. Rouleau, R. Schuch, F. Söderberg, E. Beebe, I. Bergström, A. Paal, A. Pikin, G. Bollen, H. Hartmann, R. Jertz, H-J. Kluge, T. Schwarz, P. Senne, and R. Mann, *Phys. Scr.* **T59**, 134 (1995).
- [10] G. Gräff, H. Kalinowsky, and J. Z. Traut, *Phys. Acoust.* **297**, 35 (1980).
- [11] C. Carlberg, T. Fritioff, and I. Bergström, *Phys. Rev. Lett.* **83**, 4506 (1999).
- [12] T. Fritioff, C. Carlberg, G. Douysset, R. Schuch, and I. Bergström (private communication).
- [13] S. Brunner, T. Engle, A. Schmitt, and G. Werth, in *Trapped Charged Particles and Fundamental Physics* (Ref. [6]), p. 125.
- [14] S. R. Jefferts, Ph.D. thesis, University of Colorado, 1992, available through University Microfilms International, Dissertation Copies, P.O. Box 1764, Ann Arbor, MI 48106. Order Number AAC9232697.
- [15] S. R. Jefferts, T. Heavner, P. Hayes, and G. H. Dunn, *Rev. Sci. Instrum.* **64**, 737 (1993).
- [16] T. P. Heavner, M. Zuo, P. Hayes, S. R. Jefferts, and G. H. Dunn, *Phys. Scr.* **T59**, 414 (1995).
- [17] T. P. Heavner, Ph.D. thesis, University of Colorado, Boulder, 1998, available through University Microfilms International, Dissertation Copies, P.O. Box 1764, Ann Arbor, MI 48106. Order Number AAG9827720.
- [18] L. S. Brown and G. Gabrielse, *Rev. Mod. Phys.* **58**, 233 (1986).
- [19] R. M. Weisskoff, Ph.D. thesis, Massachusetts Institute of Technology, Cambridge, MA, 1988.
- [20] D. J. Wineland and H. G. Dehmelt, *Int. J. Mass Spectrom. Ion Phys.* **16**, 338 (1975).
- [21] F. L. Moore *et al.*, *Phys. Rev. A* **46**, 2653 (1992).
- [22] G. Audi and A. H. Wapstra, *Nucl. Phys. A* **595**, 409 (1995).
- [23] S. G. Lias *et al.*, *J. Phys. Chem. Ref. Data Suppl.* **17**, (1988); *CRC Handbook of Chemistry and Physics, 74th Edition, 1993–1994*, edited by D. R. Lind (CRC, Boca Raton, FL 1993), pp. 10–205.
- [24] R. S. Van Dyck, Jr., *Proceedings of the International Conference On Nuclei Far From Stability and Ninth International Conference on Atomic Masses and Fundamental Constants 1992*, edited by R. Neugart and A. Woehr (Institute of Physics, Bernkastel, 1993), p. 3.